The Advanced Geared Turbofan 30,000 lb_f – electrified (AGTF30-e): A Virtual Testbed for Electrified Aircraft Propulsion Research

Jonathan L. Kratz*
NASA Glenn Research Center, Cleveland, Ohio, 44135, U.S.A.

Electrified Aircraft Propulsion (EAP) is a growing topic of research with the potential to shape the future of commercial air travel. Here, detailed mathematical models serve an essential role in developing understanding and evaluating different technologies and design concepts. The Advanced Geared Turbofan 30,000lb_f – electrified (AGTF30-e) is an open-source software package developed by the National Aeronautics and Space Administration (NASA). The AGTF30-e provides a realistic propulsion system model of a conceptual electrified advanced geared turbofan engine suitable for propelling a single-aisle commercial aircraft. Included with the engine model is a controller that provides representative dynamic performance across a full operating envelop. The model is meant to facilitate research studies and promote collaboration. It is envisioned for use in concept exploration studies, technology impact studies, and dynamics and controls studies. The engine model can be run in various modes of operation including boost and power extraction. It also has options for other electrification features and methods for engine shaft and electric machine integration. This paper documents the AGTF30-e and illustrates its use through various simulation scenarios.

I. Introduction

System studies, dynamic analysis, and control studies are key features of fundamental research, technology evaluation, and preliminary concept development. In the early stages of research, it is valuable to develop an understanding of the governing physics, parameter sensitivities, and the benefits and challenges associated with the new technologies and concepts being considered. The practice of modeling and simulation is a common and relatively quick and cost-effective approach to obtaining this understanding. Electrified Aircraft Propulsion (EAP) has emerged as a promising area of research with the primary goals of reducing fuel consumption, emissions, and noise associated with flight [1]. The practice of modeling and simulation has played a key role in EAP research and will continue to do so.

The National Aeronautics & Space Administration (NASA) has a legacy of developing models to support fundamental research and to investigate the utility of new technologies. In particular, the NASA Glenn Research Center (GRC) has a background in propulsion system modeling that goes back decades. The initial development of dynamic engine performance simulations was achieved in the early 1950's through use of electronic analog computers at the National Advisory Committee of Aeronautics (NACA) Lewis Research Center (now NASA GRC) [2]. The Numerical Propulsion System Simulation (NPSS) code was developed by NASA GRC in 1995 as acknowledged by the Southwest Research Institute (SwRI) who currently controls the code maintenance and development†. NPSS is a modular and extensible framework for the integration of multicomponent and multidisciplinary analysis tools written in the C/C++ language [3]. It is a widely used tool for developing models of air-breathing engine systems. In 2014, NASA GRC released the Toolbox for the Modeling and Analysis of Thermodynamic Systems (T-MATS) [4]. T-MATS brings some of NPSS's capabilities into the MATLAB/Simulink® coding environment, which is convenient for transient simulation and control design. Soon after the release of T-MATS, the software was leveraged by NASA to develop the Advanced Geared Turbofan 30,000 lb_f (AGTF30) [5]. The AGTF30 is a generic engine model

* Research Engineer, Intelligent Control & Autonomy Branch, AIAA senior member.
† https://www.swri.org/industry/aerospace-software/about-npss

representative of a NASA N+3 propulsion system concept that represents a standalone engine [6]. The purpose of the model is to facilitate transient analysis and control related research both inside and outside of NASA.

The Advanced Geared Turbofan 30,000 lb_f - electrified (AGTF30-e) is a recent addition to NASA's legacy of model development. It shares a similar goal to the AGTF30; to facilitate research studies and promote collaboration though the availability of a generic system level model with relevant features. The AGTF30-e is a transient engine model and controller that builds upon the AGTF30 with the addition of various new options and electrification features. Given that the AGTF30-e leverages the AGTF30, it too utilizes T-MATS and MATLAB/Simulink®. Like the AGTF30, the AGTF30-e is envisioned to be a good virtual testbed for research efforts. The model can be used as is or can be modified by the end-user to facilitate their specific research interests.

The rest of this paper is committed to describing the AGTF30-e and demonstrating its use through various simulation scenarios. The AGTF30-e will be clearly differentiated from the AGTF30, and the simulation results will demonstrate the specific features of the AGTF30-e. Section II provides additional information about the AGTF30 to educate the reader about the foundation upon which the AGTF30-e was built. Section III will identify the most significant changes and additions made to the AGTF30 to create the AGTF30-e. Section IV presents simulation results that demonstrate the various features of the model and highlight some of the benefits the features could bring to commercial aviation. Finally, Section V provides some conclusions and comments about potential uses for the model.

II. Background on the AGTF30

The AGTF30, depicted in Fig. 1, is a model of a geared turbofan capable of producing approximately 30,000 lb_f of thrust at sea level static (SLS) conditions. The AGTF30 is conventional in the sense that it is a standalone engine without electrification. Its key features are a compact core that promotes higher thermodynamic efficiency and a variable area fan nozzle (VAFN) that enables lower fan pressure ratio and higher propulsive efficiency. The AGTF30 is a transient engine model that accounts for shaft dynamics due to inertia. Given that the AGTF30 is modeled using T-MATS, which uses similar techniques to NPSS, it yields a system that is quasi-steady-state and 0-dimenional (non-spatial). This approach assumes the gas path dynamics to be substantially faster than the shaft dynamics that tend to dominate the transient behavior. Thus, the gas path is assumed to be quasi-steady-state. The system model is non-spatial in the sense that the component-level models provide flow property approximations at the inlet(s) and outlet(s) but do not capture spatial variations within the component. However, thermodynamic relationships and gas dynamics are captured in the modeling approach. Turbomachinery components are based on performance maps that define how parameters such as efficiency and pressure ratio relate to corrected flow rate and corrected shaft speed. An iterative Newton-Raphson solver is used to enforce conservation laws.

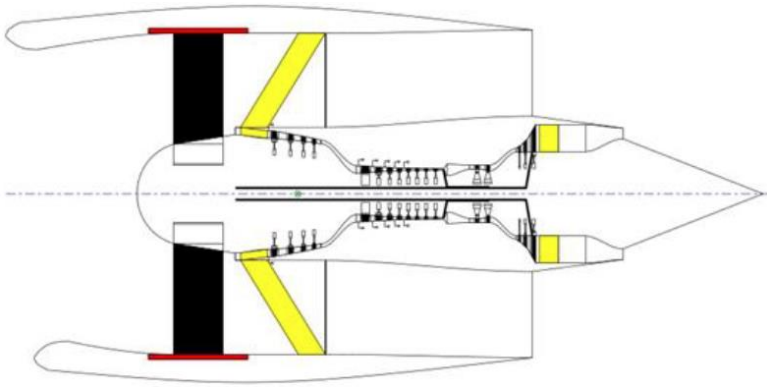

Figure 1. Representation of the AGTF30 [6].

The AGTF30 is equipped with a baseline controller that provides representative transient performance and control throughout the flight envelope. The control consists of scheduled actuators and a closed-loop proportional integral (PI) fuel flow control. Each sensor and actuator are modeled with their own dynamics and nonlinearities. The scheduled actuators include a variable bleed valve (VBV) and a VAFN. The fuel flow control operates upon a fuel modulation valve (FMV) and seeks to achieve a desired corrected fan speed that correlates with thrust. The fuel control set-point is determined by the pilot's throttle command via the power lever angle (PLA). The fuel flow control is also constrained by various steady-state and transient limits. Limiters protect against potentially unsafe or damaging conditions such as compressor stall, over-speed, over-temperature, over-pressure, and minimum operating pressure. A min-max control logic is used to decide which control is presently active and integral wind-up is implemented to protect inactive controllers from accumulating an excessive amount of error.

Since the AGTF30 was released in 2016, it has been used in numerous studies. Some of those studies are captured in Ref. [7-21]. Topics of the research include thermal analysis and distributed engine control, tip clearance control,

transient operability and control studies, gas turbine engine electrification, fault analysis, secondary flows, and hardware-in-the-loop simulation studies. Given the trajectory toward engine electrification, the incorporation of electrification features are of specific interest. While several studies have been conducted by NASA with the AGTF30 that includes the integration of an electrical power system model [9-13,16-18], no such updates have been made publicly available until the AGTF30-e.

III. Features of the AGTF30-e

The primary changes to the AGTF30 relate to the presence of an electrical power system that could be used to alter the engine operation, and the means of integrating those electrical power system components with the AGTF30 engine. The modifications were motivated by EAP research, including specific topics that have been investigated at NASA GRC. Before describing the new features of the AGTF30-e, some background is provided to give context as to why the features were targeted.

There are a variety of EAP architectures of interest, several of which are discussed in Ref. [1]. EAP concepts that interface electric machines (EMs) with turbofan engines are of particular interest. Parallel hybrid concepts such as the NASA/Boeing Sugar Volt [22] and partially turboelectric concepts such as the NASA Single-aisle Turboelectric AiRCraft with Aft Boundary Layer propulsor (STARC-ABL) [23] are examples of such architectures. In the former example, EMs and electrical energy storage are leveraged to augment the thrust of the engine during key flight segments. This feature will be referred to as boost. In the later example, EMs are used to extract power from turbofans and apply that power to drive a boundary layer ingesting electric fan. This power extraction (PEx) capability enables propulsion to be distributed over the airframe in an aerodynamically beneficial manner. Both concepts are significant deviations from state-of-the-art propulsion systems that carry potential implications to engine operation.

Other electrification features include electric power transfer (EPT), Turbine Electrified Energy Management (TEEM), and in-flight charging. EPT considers how power can be transferred between the engine shafts to achieve various benefits. References [24,25] are examples from the literature that cover this topic. Of particularly interest is Ref. [24] that suggests benefits from transferring power from the low-pressure shaft (LPS) to the high-pressure shaft (HPS) during low engine power operation. The impact is the ability to hold an adequate bleed pressure while burning less fuel and reaching a lower thrust level. This would be helpful during descent and perhaps during ground operations. Ref. [26] shares a similar sentiment. It shows how the need for a VBV can be reduced or eliminated with electric power modulation, including electric power transfer from the LPS to the HPS. It also suggests how electric power modulation could be useful to improve operability and fuel consumption during low engine power segments of operation such as ground operations. TEEM is a control approach that leverages an electrical power system interfaced with turbomachinery to improve the operability of the turbomachinery [26]. It can be used during engine power transients to better maintain compressor blade-flow incidence and protect against compressor stall. It has been suggested that the ability to tightly control engine operability alleviates design constraints and can lead to lighter and or more efficient engine designs. TEEM has been the topic of several papers including Ref. [9,10,11,13]. Its implementation typically consists of using electric machines interfaced with the engine shafts to inject or extract power during transients. Energy storage can be used to source or sink electric power as needed. The typical approach calls for power injection on the HPS during accelerations, and power transfer from the LPS to the HPS during decelerations. Energy storage is a common component of electrified propulsion architectures and would be especially applicable with features such as boost and TEEM. The possibility of charging in-flight is a consideration that could impact aircraft weight and mission efficiency.

Another topic of consideration is how the EMs are interfaced with the engine shafts. The engine-EM integration method could carry implications for the shaft dynamics and how mechanical power flows through the propulsion system. By extension, the way in which the system is controlled could be impacted. An obvious method for engine-EM integration is what will be referred to in this paper as the dedicated EM (DEM) approach. In this approach, each shaft has its own EM(s) that are coupled through its own gearbox. Another option being investigated by NASA is the Versatile Electrically Augmented Turbine Engine (VEATE) gearbox concept [11]. This approach interfaces one or more EMs with both engine shafts through a single mechanical power transmission system. This will require at least three input/output paths for the gearbox, two of which interface with the engine shafts and the other with an EM. This concept enables power injection/extraction to simultaneously influence power flow through the mechanical powertrain. Depending on the design/configuration of the VEATE gearbox and the rotational speeds of the mechanical components, the EM inputs could influence mechanical power transfer between the engine shafts or adhere to a power split that funnels the power from/to the EMs to/from the engine shafts. The flexibility of leveraging mechanical power flow paths for power management opens new possibilities and points toward several potential benefits. Some of those

benefits include reduction of the size of the electrical power system, more benign failure modes and mitigation strategies, and flexibility to address integration challenges.

A. Noteworthy Changes from the AGTF30

The AGTF30-e is built upon the AGTF30 and shares many of the same features. It effectively uses the same turbomachinery performance maps and has the same scaling of those maps. The steady-state performance was characterized throughout the flight envelope and for all engine power and electric power injection/extraction combinations. Given that the same performance maps and scaling were used for the AGTF30-e as was for the AGTF30, it implies that the engine is effectively the same for all modes of operation, including boost and PEx. Thus, one can view the engine as being re-purposed for electrification applications without re-design.

While the AGTF30-e and AGTF30 have matching performance for the same actuator inputs, the AGTF30-e maximum and minimum engine power conditions could differ, and the AGTF30-e engine power range is generally larger. The AGTF30 and AGTF30-e also have a different set of limiters. While some limits, such as the maximum turbine inlet temperature, are the same, other limiters are different and the AGTF30-e considered additional limiters, such as the maximum HPC discharge temperature. In general, without any electrification options enabled, the AGTF30-e tends to reach a similar maximum thrust and a lower minimum thrust than the AGTF30 does.

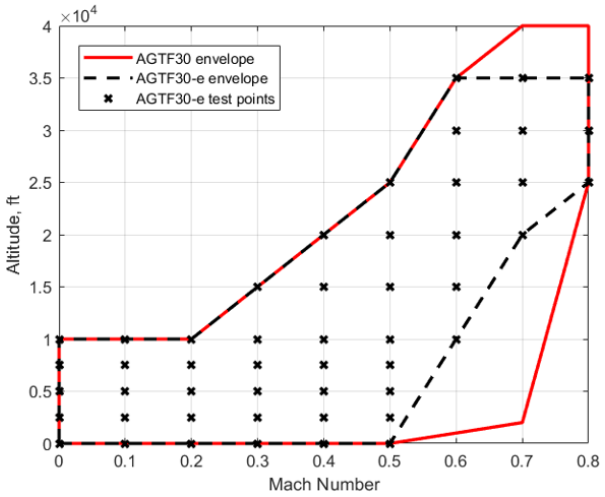

Figure 2. AGTF30-e flight envelope.

The development of the AGTF30-e called for added complexity in a number of ways, all of which added to the difficulty and duration of development. To help keep the development effort practical, the flight envelope of the AGTF30 was shrunk for the AGTF30-e. Figure 2 compares the two flight envelopes. The "x's" indicated that points at which steady-state analysis, control design, and model testing were conducted.

The AGTF30 assumed a constant power extraction of 350 hp from the HPS for the purpose of powering engine and aircraft subsystems. The AGTF30-e allows for the aircraft load to change through the mission. The nominal power extraction is assumed to be 175hp.

B. Primary Electrification Options

The AGTF30-e can represent a conventional non-electrified engine. It can also operate with boost and PEx. The user can specify which electrification option they wish to simulate. The conventional engine option is the option most similar to the AGTF30. With this option, there is no boost and no PEx beyond what is required for the aircraft subsystems (nominally 175 hp of power extraction). Boost mode will allow up to 2000 hp of power injection to the LPS. Even while boost mode is enabled, a toggle switch command can be prescribed by the user to enable or disable the boost feature. This allows the boost feature to be enabled only when it is advantageous for the mission at the discretion of the pilot. The PEx mode calls for up to 1000 hp of power extraction from the HPS and up to 750 hp of PEx from the LPS. The 1000hp of PEx from the LPS includes the aircraft load allotment (nominally 175hp). Thus, up to 825 hp is extracted from the HPS to produce thrust elsewhere on the airframe. The amount of power injection for boost and power extraction for PEx mode was determined during the steady-state analysis phase of the model's development. It was found that these power levels for boost and PEx were close to the maximum of what could be sustained throughout a significant portion of the flight envelope, including top of climb and cruise conditions. Beyond these levels of power injection or extraction, the model could encounter convergence issues.

C. Secondary Electrification Options

EPT, TEEM, and in-flight charging are 3 electrification options that can be enabled in combination with each other and the 3 modes of electrification mentioned in Section III.B. Here, EPT refers to the transfer of power between the engine shafts at the low end of the engine power range. The potential benefit that is the focus of the EPT implementation in this model is the ability to reduce thrust and fuel consumption during descent and ground operations

while maintaining adequate minimum pressure to support engine bleeds. By default, enabling EPT will result in an electrical power transfer of up to 250 hp. The EPT feature can be enabled or disabled during a simulated mission/scenario. TEEM is enabled or disabled prior to a simulation. TEEM will call for power injection to the HPS during accelerations and power transfer from the LPS to the HPS during decelerations. The effect is improved transient operability for the compressors. The in-flight charging option can be enabled or disabled during a simulated mission/scenario. This allows the charging feature to be utilized when it is most advantageous or necessary at the discretion of the pilot. When enabled, the charging feature will allow for additional power extraction or injection to achieve and maintain a desired state of charge (SOC) of the energy storage device.

D. Engine – Electric Machine Integration Options

Two options are available for integrating EMs with the engine shafts. The first is the DEM approach which is straight-forward to visualize (see Fig. 3). In this approach, each EM would be directly coupled to an engine shaft without any mechanical connection (other than bearings) leading to the other shaft. Each EM would be interfaced with the engine shaft through a gearbox that has a fixed gear ratio, and thus a fixed speed ratio between the EM and engine shaft. An energy storage system can be used to facilitate power management between the two EMs.

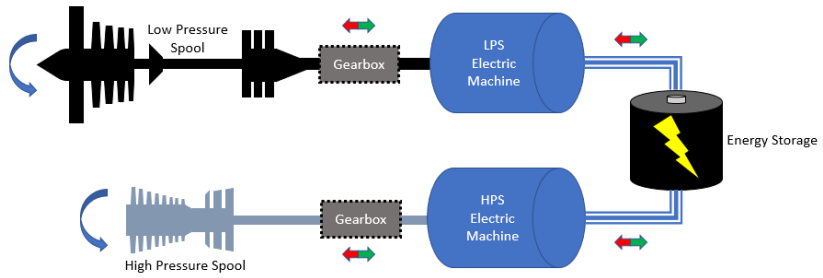

Figure 3. Illustration of the DEM approach. Components with dashed outlines are optional. Arrows indicate the direction of power flow. Red arrows indicate EM power addition into the shaft and green signifies extraction from the shaft.

The second option is the VEATE gearbox option (see Fig. 4). The non-trivial nature of this approach requires some additional explanation, and that will be the focus for the remainder of this sub-section. With this option, a planetary gearbox (PGB) variant of a VEATE gearbox is implemented to interface EMs with both engine shafts. Figure 5 shows a simple representation of a planetary gearbox and identifies the main components. The sun gear, ring gear, and carrier are the primary input-output components, and the planet gears rotate about axles connected to the carrier and between the sun and ring gears to which they mesh. A VEATE PGB would interface 2 of the primary components with the engine shafts while the other is interfaced with an EM. This EM will be referred to as the coupling EM because its usage produces a coupling effect between the shafts. Figure 6 shows an example of a VEATE PGB configuration with the sun gear interfaced with the HPS and the

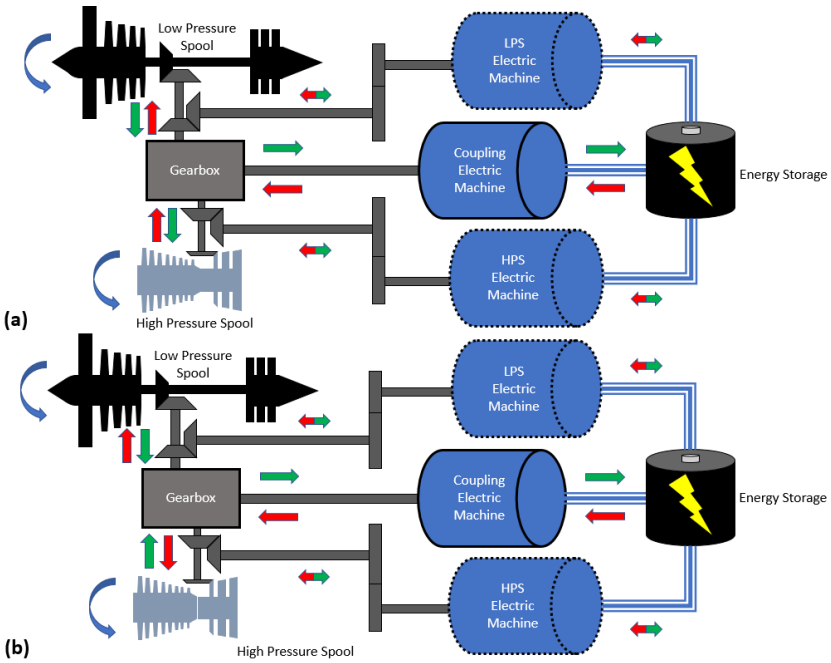

Figure 4. Illustration of the VEATE gearbox approach with a configuration that influences (a) power transfer and (b) a power split between the shafts. Components with dashed outlines are optional. Arrows indicate the direction of power flow. Red arrows indicate EM power addition and green signifies extraction.

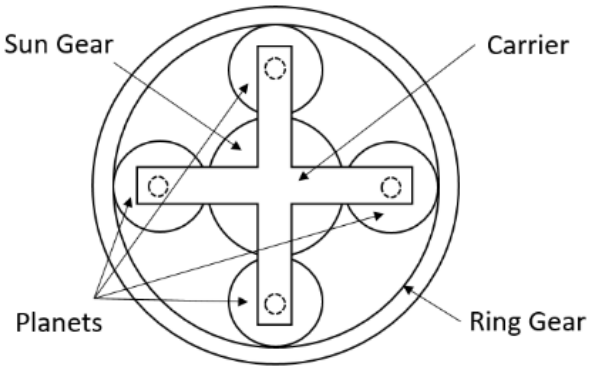

Figure 5. Simple representation of a planetary gear

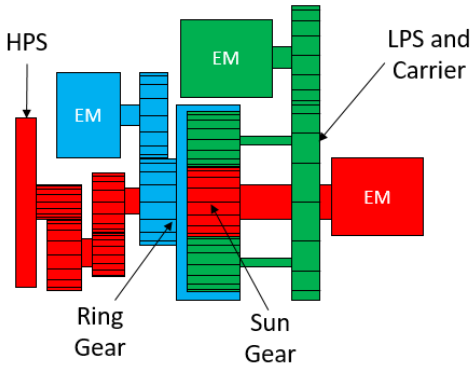

Figure 6. Representation of a VEATE PGB.

carrier interfaced with the LPS. The coupling EM is attached to the ring gear. Depending on the design/configuration of the gearbox, the coupling EM power could be split between the engine shafts, or it could influence power transfer between the shafts. EMs may also be interfaced to the engine shafts or geartrains connected to the engine shafts as shown in Fig. 4. The arrangement can be tailored for a desired impact. The VEATE PGB option allows for a spectrum of different EM inputs that achieve the same result as experienced by the engine shafts. While the effect is the same, there are potential benefits with respect to power system size and flexibility of integration, failure mitigation, and more.

The effect of the gearbox is determined by the gearbox arrangement (which components are connected to the engine shafts), relative gearbox component sizes (sun gear to ring gear radius ratio and various gear ratios), and the relative inertias of the components. These factors also help determine the relative speeds and direction of rotation of the gearbox components, which can impact the flow of power. The acceleration of the shafts (and the gearbox components to which they are connected/interfaced) is given by the equation below, neglecting losses.

$$\dot{N} = \frac{60}{2\pi}\frac{1}{J_{Eff}}\sum \tau \tag{1}$$

$\dot{N}$ is the shaft acceleration in rpm, J_{Eff} is the effective inertia in slug-ft^2 and τ is the torque on the shaft in ft-lb$_f$. The effective inertia accounts for the reflected inertia of all relevant components. This equation can be written out for any rotating component in the mechanical powertrain. For the PGB components, the acceleration of each component can be written out as a function of the torques applied at each PGB component multiplied by a constant that is a function of the gearbox design parameters (gear radii, number of planets, and the mass of planets) and component inertias. Eq. (2) provides an example for the sun gear where C_{sr}, C_{sc}, and C_{sp} are torque coefficients that determine how effective torques applied at the ring gear, carrier, and planetary gears are at manipulating the sun gear.

$$\dot{N}_s = \frac{60}{2\pi}\frac{1}{J_{Eff,s}}\left(\tau_s + C_{sr}\tau_r + C_{sc}\tau_c + C_{sp}\tau_p\right) \tag{2}$$

The subscripts *s*, *r*, *c*, and *p* are for the sun gear, ring gear, carrier, and planet gears. The coefficients of the form C_{xy} determine how torque applied at component *y* translates to torque applied at another component *x*, where the subscripts *x* and *y* can be *s r*, *c*, or *p* as defined above. As mentioned prior, these coefficients are strictly functions of physical gearbox parameters that should be known once the design is set. Similar equations can be written for the ring gear and carrier. Given the rigid fixed gear ratio connection between the engine shafts and the PGB components to which they are interfaced, the expressions can be related to engine shaft accelerations as well. Casting Eq. (2) in terms of power, *P* (expressed in hp), brings in the relevance of the gearbox component speeds N_s, N_r, N_c, and N_p given in rpm. Eq. (3) shows an example.

$$\dot{N}_S = 550\left(\frac{60}{2\pi}\right)^2\frac{1}{J_{Eff,S}}\left(\frac{1}{N_s}P_s + \frac{C_{sr}}{N_r}P_r + \frac{C_{sc}}{N_c}P_c + \frac{C_{sp}}{N_p}P_p\right) \tag{3}$$

The effectiveness of power addition or extraction through the other gearbox components is determined by the coefficient C_{xy} and the relative speeds of the components N_x and N_y. The Appendix provides expressions for the torque coefficients and effective inertias of each PGB component.

When C_{xy}/N_y is positive, addition of power through component *y* will result in power addition to component *x*. If component *y* is the coupling component and $0 < C_{xy} < 1$, the power applied/extracted to/from component *y* would be split between the engine shafts. If $C_{xy} > 1$ then the power from component *y* goes to component *x* and it results in additional power to the shaft interfaced with component *x* through mechanical power transfer from the shaft connected to component *y*. When C_{xy}/N_y is negative, addition of power through component *y* will result in power extraction from component *x*. If component *y* were the coupling component, the result would be power transfer from the shaft connected to component *x* to the other engine shaft.

With the PGB effect better understood, one can appreciate how the gearbox design will impact mechanical power flow through the system and how it can be calculated for control allocation. With the VEATE PGB option enabled, the AGTF30-e replaces the T-MATS shaft blocks with a dynamic planetary gearbox that computes the shaft accelerations. The gearbox model assures that the velocity of the gearbox components at their interfaces is the same and that gear tooth forces at the interfaces are equal and opposite.

The default VEATE gearbox option of the original AGTF30-e release implements a PGB interface solution that integrates the sun gear with the HPS and the carrier with the LPS. This makes the ring gear the coupling component. C_{sr} is chosen to be negative while this will make C_{cr} positive and greater than 1. This means that power injection with the coupling EM will add power to the LPS and influence mechanical power transfer from the HPS to the LPS, further boosting the LPS. Power extraction with the coupling EM would have the opposite effect. This approach was taken because it is thought to be the most advantageous for the applications in mind (boost, power extraction, EPT, and TEEM). For EPT, power extraction with the coupling EM and power injection with an EM connected to the HPS will enhance the engine spool power transfer effect. For TEEM, power extraction with the coupling EM during accelerations will boost the HPS and supplement the power addition provided by the HPS EM. In some applications, this may allow the HPS EM to be reduced in size and it could allow the TEEM energy storage system to be reduced in size as well through leveraging the power transfer effect of the VEATE gearbox during accelerations. During decelerations, the mechanical power transfer effect will reduce the amount of power transfer needed to be accomplished through the EMs. This could help reduce the size of the power system, enhance the operability benefit observed, and or improve engine responsiveness during deceleration transients. For boost, power injection with the coupling EM will boost the LPS while influencing power transfer from the HPS to the LPS. This means that more power can be injected on the HPS rather than directly on the LPS. Given that the HPS spins faster, and an EM interfaced with the HPS may also spin faster, it might be possible to inject power at a lower torque which correlates to a lower EM weight than if that power were injected directly onto the LPS. This solution may also spread the EM power out more evenly across multiple machines and leverage a mechanical power flow path between the engine shafts that could have advantages with respect to failure modes and failure mitigation. Similar benefits could be possible with the PEx application. Power extraction with the coupling EM will influence power transfer from the LPS to the HPS, thus allowing more of the power extraction to occur on the HPS. Given the promising attributes of this configuration, some aspects of the EM controllers with the VEATE option assume the power transfer effect described above. This has implications on what the physical parameters of the gearbox can be. If this condition is not met, the controller may not behave as desired and changes to the control approach could be necessary.

E. Electrical Power System

The electrical power system consists of multiple electrical machines, inverters/rectifiers, cables, a DC-DC converter and a generic energy storage device. The model has performance maps for the EMs and constant efficiencies for other components. By default, the efficiencies are set to 100%. It is possible that a future update of the model could add realism by incorporating losses in the electrical power system. However, that was outside the scope of the effort for the initial release. Assuming 100% efficiencies simplified the model creation process by not having to account for the losses in the power flow book-keeping and it alleviates the need to address complications that it might impose on the controller for state of charge regulation. For the PEx option, the load consumed by the external propulsor(s) is assumed to be equivalent to what is commanded by the controller, and this is accounted for in the power system model.

F. Versatile Control Implementation

The AGTF30-e comes with a baseline controller that implements the many features of the model. It has logic for enforcing default power injection/extraction schedules, conventional engine controls (fuel flow rate, VBV, VAFN), and has methods for implementing EPT, TEEM, and in-flight re-charging. Beyond the default control settings, the controller has the ability to accommodate changes in boost and PEx power schedules. It can also accommodate

changes in shaft inertias that could result from the addition of EMs and the impact of the engine-EM interface solution. The following paragraphs provide a high-level description of the control approaches.

The AGTF30-e has open-loop actuator schedules for the VBV and VAFN. The schedules are functions of pressure--altitude, Mach number, corrected fan speed, and power injection/extraction from the engine shafts. The fuel flow controller is a closed-loop controller with min-max limit protection [27]. The corrected fan speed set-point is determined by a lookup table that considers the pressure-altitude, Mach number, power injection/extraction, and throttle position. Steady-state limits are enforced through the min-max approach, and they adjust the set-point value to prevent limit violations. Acceleration, deceleration, and minimum fuel flow rate limits are enforced by directly limiting the fuel flow rate command through min-max decision logic. The nominal fuel flow command is calculated using a gain scheduled PI controller. Each steady-state limit controller commands a corrected fan speed set-point through a gain scheduled PI controller. All PI controllers have integral windup protection to prevent excessive error accumulation while the controllers are inactive. The minimum fuel flow rate limit is determined by a look-up table, and acceleration and deceleration limiters are enforced through ratio unit (*RU*) schedule that relates the maximum or minimum ratio unit to the pressure-altitude, Mach number, and corrected fan speed. The *RU* is the quotient of the fuel flow rate divided by the static discharge pressure of the HPC. The *RU* schedules are different for each of the primary modes of electrification such that differences in the power schedule are accounted for. Alternative acceleration and deceleration limit logic exist in the form of a direct fuel flow rate limiter that limits the change in the fuel flow rate command from one time-step to the next based on an exponential response from the current fuel flow rate to prescribed maximum and minimum fuel flow rate values [28]. This approach is less realistic for implementation and transient performance is less desirable. However, it does provide a generic means of achieving representative results without redesigning the *RU* schedules when changes that impact transient performance are introduced. This could include significant changes in effective shaft inertias or variations in the power schedule employed for boost or PEx. Given that the VBV and VAFN schedules and controller gain schedules accommodate variations in power injection/extraction, the model is robust to changes in the boost and PEx power schedules. The model is also adaptable to changes in the EPT and charging logic. In addition, the control gains for the fuel flow rate controller were designed for a range of shaft inertias, which should help to assure adequate controller performance if changes in inertia are made. The effective inertia range for the LPS is 17.44 to 26.16 slug-ft^2 and the HPS inertia can vary from 1.86 to 5.58 slug-ft^2.

The boost power schedule is determined similar to Ref. [28]. The boost power P_B is calculated with Eq. (4) where P_{max} is the maximum boost power, φ_P is a scaler for the engine power level, φ_{SOC} is a scaler for the SOC, and φ_{TS} is a scaler for the boost toggle switch.

$$P_B = P_{max}\varphi_P\varphi_{SOC}\varphi_{TS} \tag{4}$$

The value of each scaler is between 0 and 1. The value of φ_P and φ_{SOC} is determined using the schedules plotted in Fig. 7. The parameter $\bar{N}_{1c}$ is the normalized corrected fan speed, which scales the corrected fan speed between the minimum and maximum corrected fan speed for the current conditions (pressure-altitude and Mach number) to values between 0 and 1. The value of φ_{TS} is zero when the boost toggle switch is off, and it is 1 when it is on. However, a rate limiter prevents this transition from happening instantaneously. The transition occurs through a 10 s ramp. When the DEM approach is used, all the power is input on the LPS via the LPS EM. When the VEATE option is enabled, a portion of the boost power will be applied by the coupling EM and the EM interfaced with the HPS. The boost power command for each EM will be determined with knowledge of how the application of power with the coupling EM impacts the engine shafts. The coupling EM will be used as much as possible or as needed, which ever results in a lower power input. The remaining power desired for addition to the LPS is provided by the EM most closely interfaced with it. Because power is transferred from the HPS to the LPS through the effect of the coupling EM, some power must be added to the HPS to achieve the expected engine operating conditions.

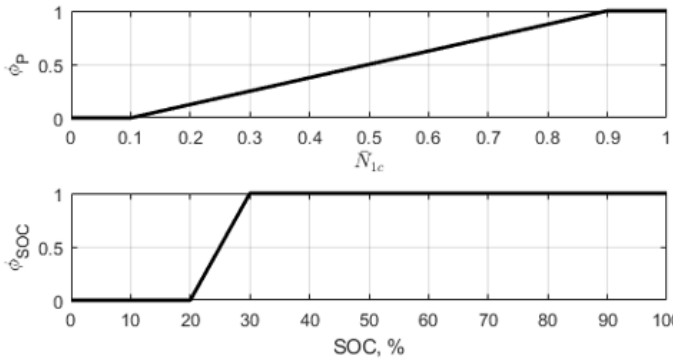

Figure 7. Plot of scaler schedules for boost power determination

The PEx power and HPS/LPS power split is a function of pressure-altitude, Mach number, and engine power level in the form of the normalized corrected fan speed. The maximum power extraction for propulsion purposes is plotted in Fig. 8. Figure 9 provides an example of the power extraction schedule and power split between the engine shafts for SLS conditions. For the DEM approach, the PEx power and power split schedules define the power that should be extracted by the LPS and HPS EMs. When the VEATE option is enabled, the coupling EM will be used as much as possible to leverage the power transfer effect. Knowing the impact of the coupling EM, the remaining power extraction required on the LPS and HPS can be computed and enforced by the other EMs.

EPT is enforced with the simple equation shown below.

$$P_{EPT} = P_{max}\varphi_P\varphi_{TS} \qquad (5)$$

Note that the variable names and meanings are shared with those in Eq. (4) but the values are different. Here, P_{max} is the maximum amount of power transfer. The toggle switch rate limiter applies a 5 sec ramp to promote a smooth and gradual transition in and out of EPT mode. The value of φ_P is determined with the schedule shown in Fig. 10. The φ_P parameter assures EPT is only applied at low engine power levels and transitions smoothly as the power level changes. For the DEM option, the EPT command is the amount of power that will be extracted from the LPS via the LPS EM and applied to the HPS via the HPS EM. When the VEATE option is enabled, the EPT command defines the amount of power that will be extracted with the coupling EM and applied to the HPS via the EM interfaced most closely with it. This will result in an enhanced power transfer effect and both options will result in zero net power.

The TEEM control implementation was guided by prior experiences such as Ref. [13], but a reduced

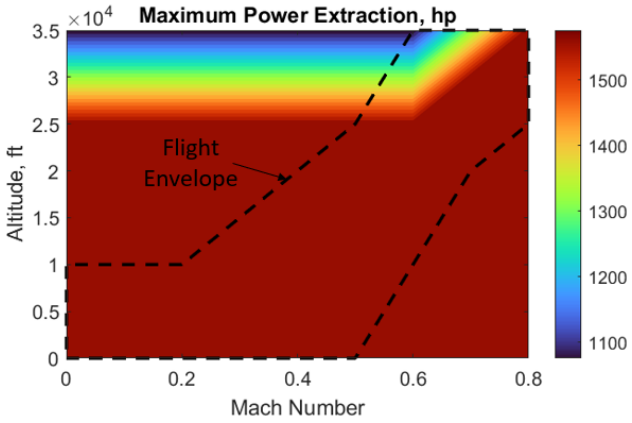

Figure 8. PEx maximum power schedule

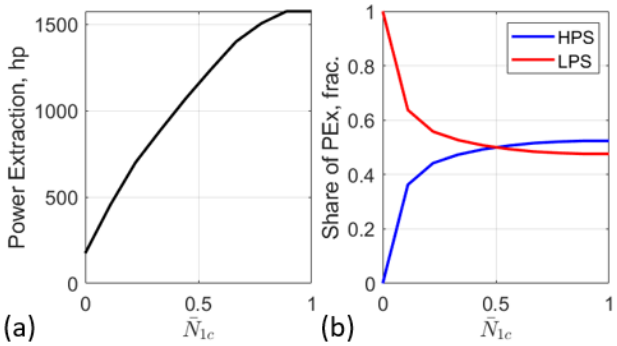

Figure 9. Example of PEx power and power split schedules at SLS conditions

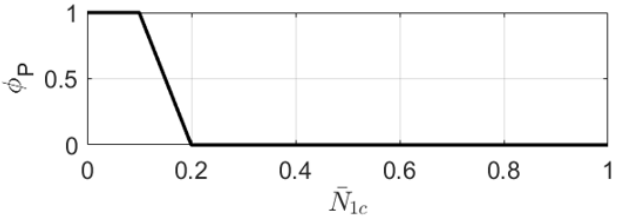

Figure 10. Engine power level scaler for EPT.

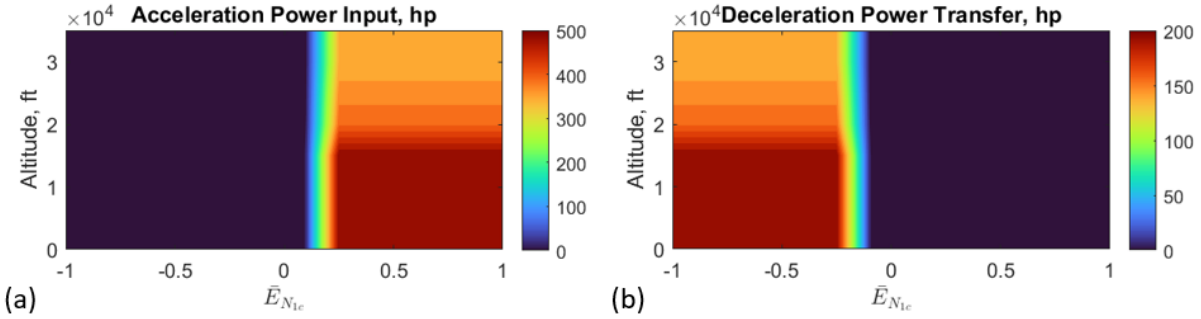

Figure 11. TEEM power schedules

amount of rigor was taken to optimize the control schedules. The supplemental power commands during the transients are determined by a power injection schedule during accelerations, and a power transfer schedule during decelerations. During accelerations, the schedule sets a target power injection to the HPS. During decelerations, the schedule sets a target power transfer via the LPS EM or coupling EM to the EM coupled most closely with the HPS. The schedules are the same for all primary electrification modes. The schedules are plotted in Fig. 11. The schedules are functions of pressure-altitude and normalized corrected fan speed error, $\bar{E}_{N_{1c}}$. $\bar{E}_{N_{1c}}$ is defined in Eq. (6) where $N_{1c,SP}$ is the corrected fan speed set-point, $N_{1c,sens}$ is the sensed corrected fan speed, and $N_{1c,Max}$ and $N_{1c,Min}$ are the maximum and minimum expected corrected fan speeds for the current flight condition.

$$\bar{E}_{N_{1c}} = \frac{N_{1c,SP} - N_{1c,sens}}{N_{1c,Max} - N_{1c,Min}} \tag{6}$$

The normalized error helps to determine if a transient is occurring and how aggressive to be with the EMs. The engine responsiveness is relaxed at higher altitudes and so the magnitude of the EM power input or transfer is also reduced. For the DEM option, the power injection schedule defines the amount of power that should be supplied by the HPS EM. The power transfer schedule defines the amount of power that is extracted from the LPS and applied to the HPS. For the VEATE option, the power injection schedule defines the amount of power that should be applied to the HPS. It will use the coupling EM as much as possible to supply the power by extracting power from the LPS and influencing mechanical power transfer to the HPS. The remainder of the power to be delivered to the HPS is supplied by the EM interfaced with the HPS. The use of the coupling EM helps to offset the power needed from an energy storage device. For decelerations with the VEATE option, the power transfer schedule defines the amount of power that should be extracted with the coupling EM and applied by the EM interfaced with the HPS. This still results in a net zero power that does use the energy storage system. It also enhances the power transfer effect, thus enhancing the operability benefit.

The charging logic commands additional power extraction or injection from/to the HPS when applicable. By default, the maximum power injection or extraction for SOC regulation is 50 hp. The SOC target is 85%. The charging command will diminish to zero as the SOC exceeds 80% and approaches 85%. If the SOC exceeds 87.5% the energy storage system will begin to apply power to dissipate the excess energy. The charging command is not applied during transients. This is enforced by multiplying the command by a scaler that is 1 for $\bar{E}_{N_{1c}}$ < 0.05 and transitions to 0 for $\bar{E}_{N_{1c}}$ > 0.1. The charging logic is enabled through the charging toggle switch. There is a 1 sec ramp applied to the toggle command, which promotes a smooth transition when enabling and disabling the charging feature.

IV. Simulation Scenarios and Results

The engine model was exercised over the flight envelope and engine power range using the input profiles shown in Fig. 12. The throttle position is represented by the power lever angle (PLA). Boost, charging, and EPT can be enabled (1) or disabled (0) via their toggle switch states. This transient simulation scenario was executed at each point

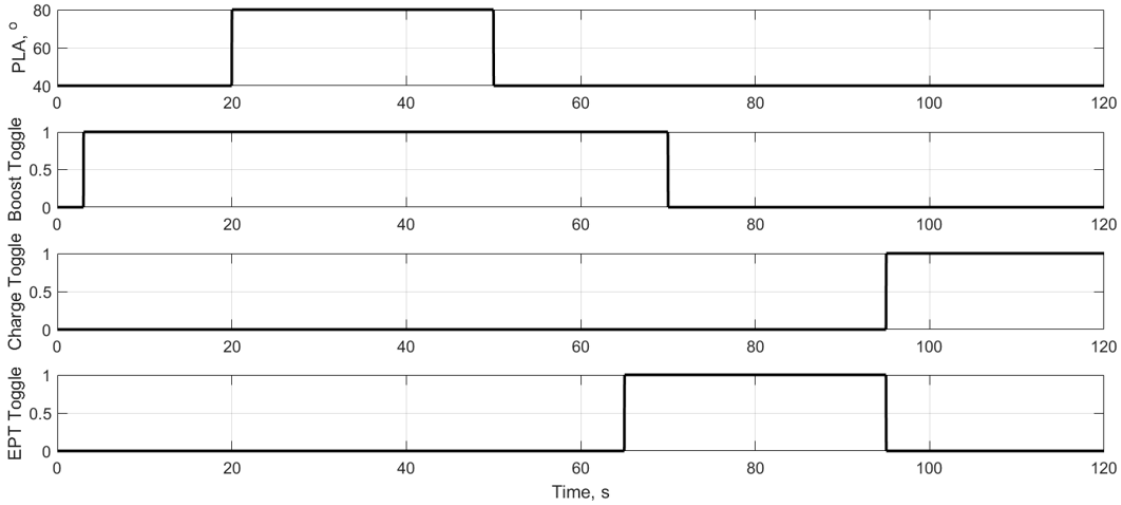

Figure 12. Model testing scenario inputs

indicated by an "x" in Fig. 2. The test scenario exercises each of the secondary electrification features when they are relevant for use. It also demonstrates operation of the engine across the engine power range and through abrupt engine power transients. The simulation scenario will start at idle power and enable boost at 3s (if applicable). At 20s a rapid acceleration is commanded through the PLA and at 50s a rapid deceleration is commanded. The boost feature (if applicable) is disabled at 70s. The EPT feature is enabled from 65s to 95s. At 95s the charging feature is enabled to replenish the energy storage system. The simulation scenario was conducted for each primary electrification option in combination with and without TEEM and each engine-EM integration option. All simulations were observed to be successful, which demonstrates the engine model and its control strategies. Results of some of those simulations are dissected in the following sub-sections.

Each of the sub-sections demonstrate the various features of the AGTF30-e. Sub-section A through C take a closer look at demonstrating the primary and secondary electrification features of the engine model as well as the engine-EM integration options. Sub-section D demonstrates the ability to modify the power schedule.

A. Primary Electrification Features

The results shown in this section illustrate the successful execution of the AGTF30-e in standard, boost, and PEx mode. The results in Fig. 13 are for SLS conditions with the DEM approach and without the use of TEEM. The plotted variables include the fuel flow rate (W_f), the electric machine powers (P_L – LPS EM power, P_H – HPS EM power), net thrust (F_n), the static HPC discharge pressure (p_{s3}), and the turbine inlet temperature (T_4). Figure 13b and 13c show the variation in EM power inputs between the 3 modes of operation. As to be expected, the engine thrust is increased with boost and decreased with power extraction (see Fig. 13d). Relative to the standard engine, the maximum thrust is increased by 8.9% with boost and decreased by 11.1% with PEx. Although it should be noted that with PEx the extracted power would be used to produce thrust elsewhere on the airframe. The PEx mode also has a lower maximum fuel flow rate due to its encountering of the over temperature limit. This could be related to the reduction in air flow.

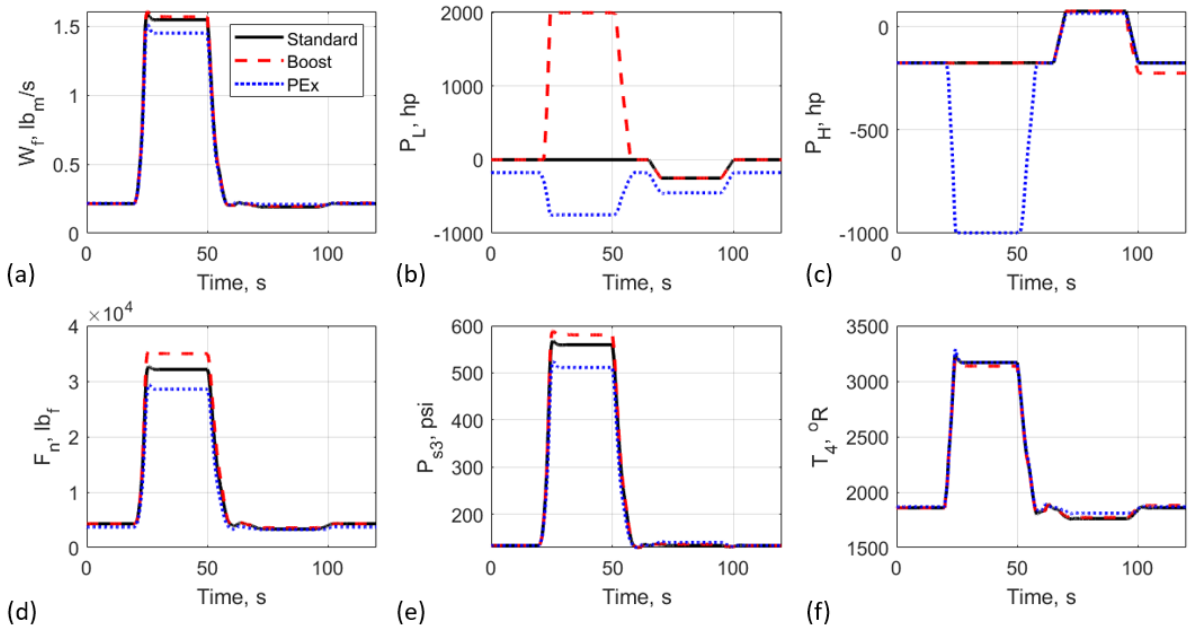

Figure 13. Results at SLS with each primary mode of electrification

B. Secondary Electrification Features

The impact of EPT is shown at SLS conditions in Fig. 14. Figure 14 zooms in on the "idle-band" of the fuel flow rate shown in Fig. 13a and distinguishes the operation with and without EPT enabled. As can be seen, the minimum fuel flow rate is reduced while the minimum p_{s3} limit is respected. For the standard engine, the minimum fuel flow rate is reduced by 11.0% relative to the minimum fuel flow rate without EPT and 1.5% relative to the maximum fuel flow rate. For boost, the improvements are 8.8% and 1.2% respectively, and for PEx they are 3.6% and 0.5%. Analysis was performed throughout the flight envelope and for the flight profile shown in Fig. 15. Because the standard and

boost options should have similar performance in the operating range in which EPT is applicable, results are only shown for the standard and PEx options. Table 1 summarizes the results. Results are shown for some key operating conditions, and the overall decrease in fuel consumption for the simulated mission scenario. The results demonstrate that that impact of EPT could be significant. Furthermore, the

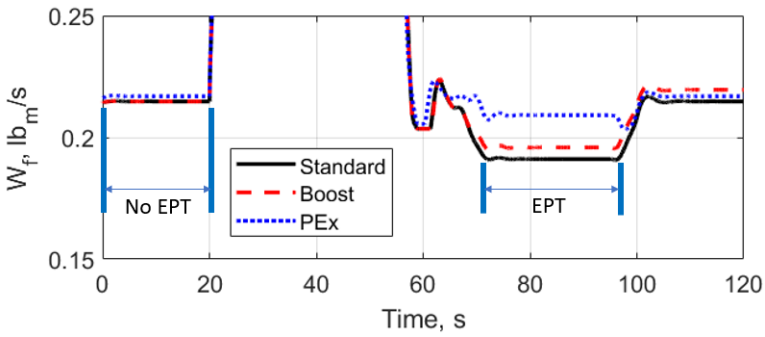

Figure 14. Impact of EPT on minimum W_f at SLS conditions

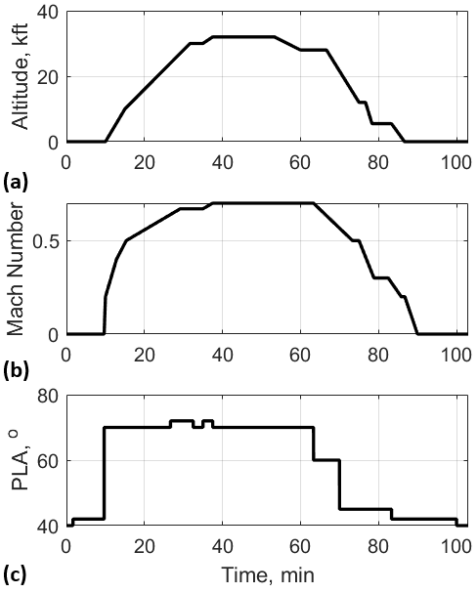

Figure 15. Full flight scenario profile

Table 1. Fuel flow impact of EPT. Fuel flow reduction is shown for idle fuel consumption at various flight conditions. The final row shows the reduction in bulk fuel consumption over the mission profile.

	Standard		PEx	
	DEM	VEATE	DEM	VEATE
0kft, Mach 0	11.03%	16.19%	3.57%	11.40%
0kft, Mach 0.2	10.14%	15.10%	2.54%	10.12%
5kft, Mach 0	12.46%	18.39%	4.16%	13.01%
5kft, Mach 0.3	10.55%	15.64%	2.86%	10.80%
10kft, Mach 0.4	11.15%	16.36%	1.50%	10.31%
15kft, Mach 0.5	10.93%	16.04%	2.30%	10.63%
20kft, Mach 0.6	10.47%	15.37%	3.45%	10.80%
30kft, Mach 0.7	12.28%	17.92%	4.89%	12.54%
35kft, Mach 0.8	13.08%	18.76%	4.88%	13.17%
Mission (Bulk W_f)	**2.73%**	**3.22%**	**1.82%**	**2.05%**
Ground benefit share	59.6%	62.9%	57.6%	62.3%
Descent benefit share	40.4%	37.1%	42.4%	38.7%

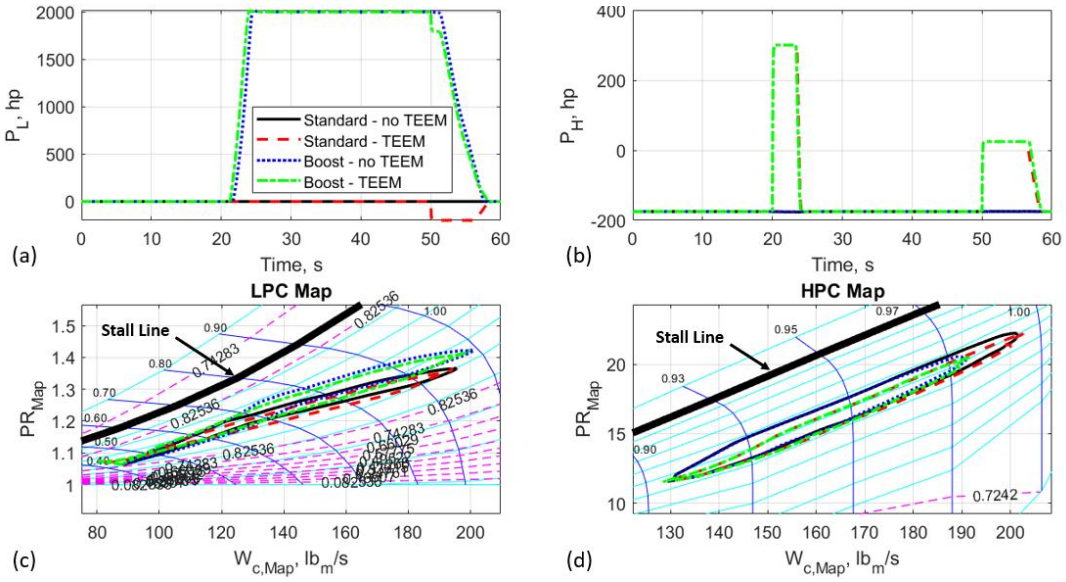

Figure 16. Impact of TEEM at SLS for the standard and boost options.

VEATE option enhances the effect. For the simulated mission, bulk fuel flow savings could exceed 3% with roughly 40% of the benefit incurred during descent and the remaining incurred during ground operations. It should be noted that these results are estimates that do not account for differences in the mission given use of EPT. The results also exhibit a slight reduction in thrust during the descent phase with EPT, which could enable a faster descent. Another noteworthy result is that the use of EPT enables the VBV area to be significantly reduced. At SLS conditions the VBV area is reduced by nearly 28%.

Figure 16 shows the EM powers as well as the LPC and HPC performance maps with transient running lines. The maps display the unscaled map corrected flow rate and pressure. The solid blue lines are constant speed lines, the dashed magenta lines are efficiency contours, and the cyan lines are r-lines used by the model solver to find a solution. Results are shown for each primary electrification mode with and without TEEM employed. When TEEM is employed an off-nominal power injection is observed during the acceleration and a power transfer between the shafts is observed during the deceleration. It is clear that the transient running lines are shifted away from the stall line, as is the goal of TEEM.

Finally, the charging feature of the AGTF30-e is demonstrated toward the end of the test scenario. Figure 17 shows the SOC variation through the simulation of the standard engine with TEEM. TEEM uses energy from the energy storage devices and when the charging feature is enabled, power is extracted from the engine and the SOC begins to increase toward the SOC set-point, as expected.

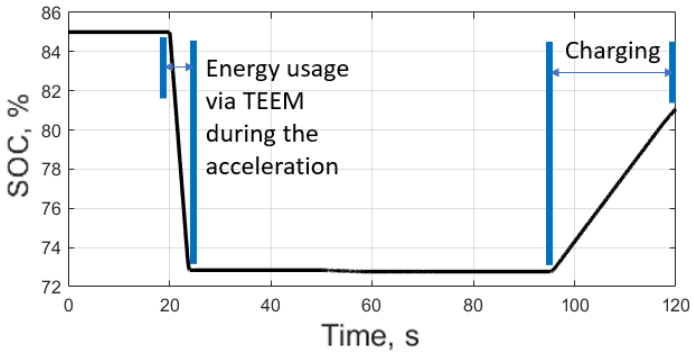

Figure 17. Demonstration of the charging logic at work.

C. Engine – Electric Machine Integration Features

In theory, the DEM and VEATE approaches should produce the same results (with some exceptions), while the EMs are used differently. The DEM and VEATE approaches are compared at the SLS condition in Fig. 18 and 19 for the PEx option. Apart from subtle differences in performance during transients and when EPT is enabled, the DEM and VEATE options produce the same results. The EM inputs are very different as shown in Fig. 18, but the fuel flow rate, thrust, and LPS and HPS speeds are the same. This provides evidence that the VEATE gearbox impact is understood and is implemented correctly. Differences observed during transients and EPT are related to differences in control implementation, which enhances the TEEM and EPT impacts with the VEATE option.

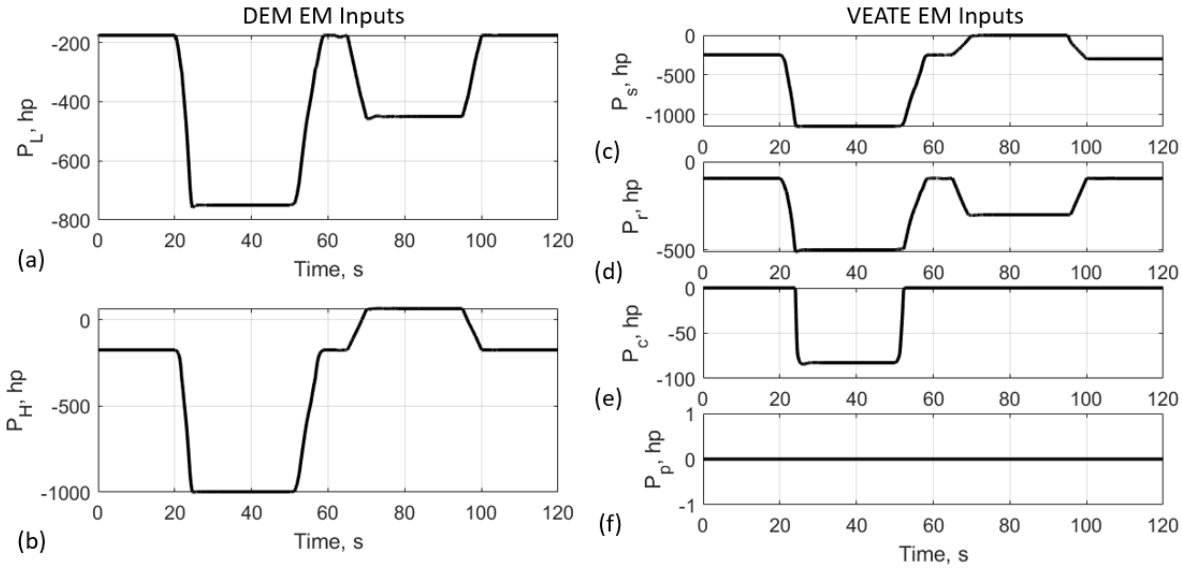

Figure 18. DEM-VEATE comparison: EM inputs

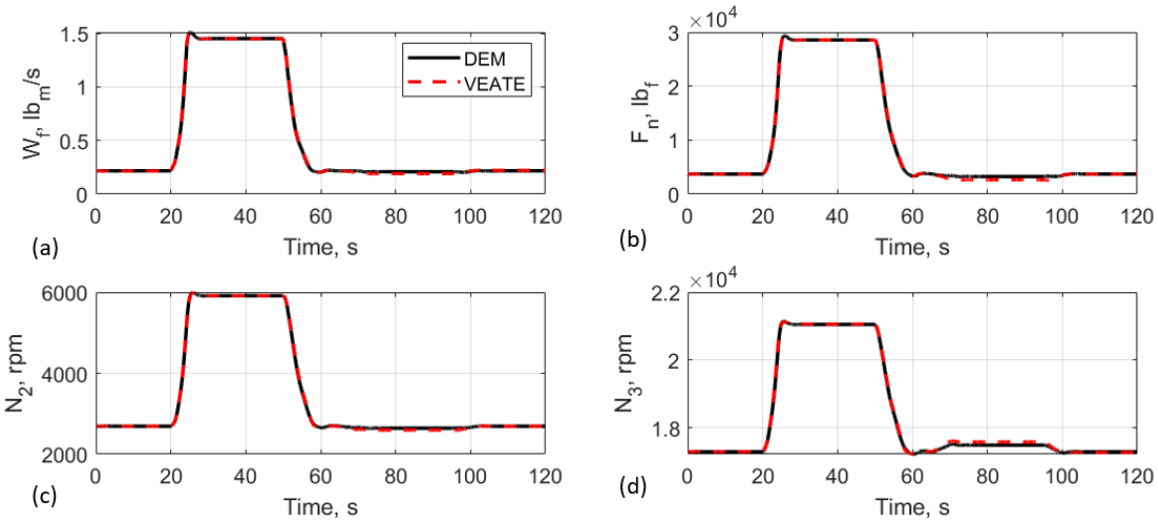

Figure 19. DEM-VEATE comparison: fuel flow rate, thrust, and shaft speeds

D. Modified Power Schedule

The power schedules for boost and PEx can be easily changed without requiring extensive controller redesign. In this example, the boost schedule was modified to inject a maximum of 1341 hp (1MW) instead of 2000 hp (~1.5MW). The PEx schedule was modified to only extract 75% of the power that the original schedule demands. To assure the acceleration and deceleration schedules do not undesirably limit the fuel flow rate and alter steady-state performance,

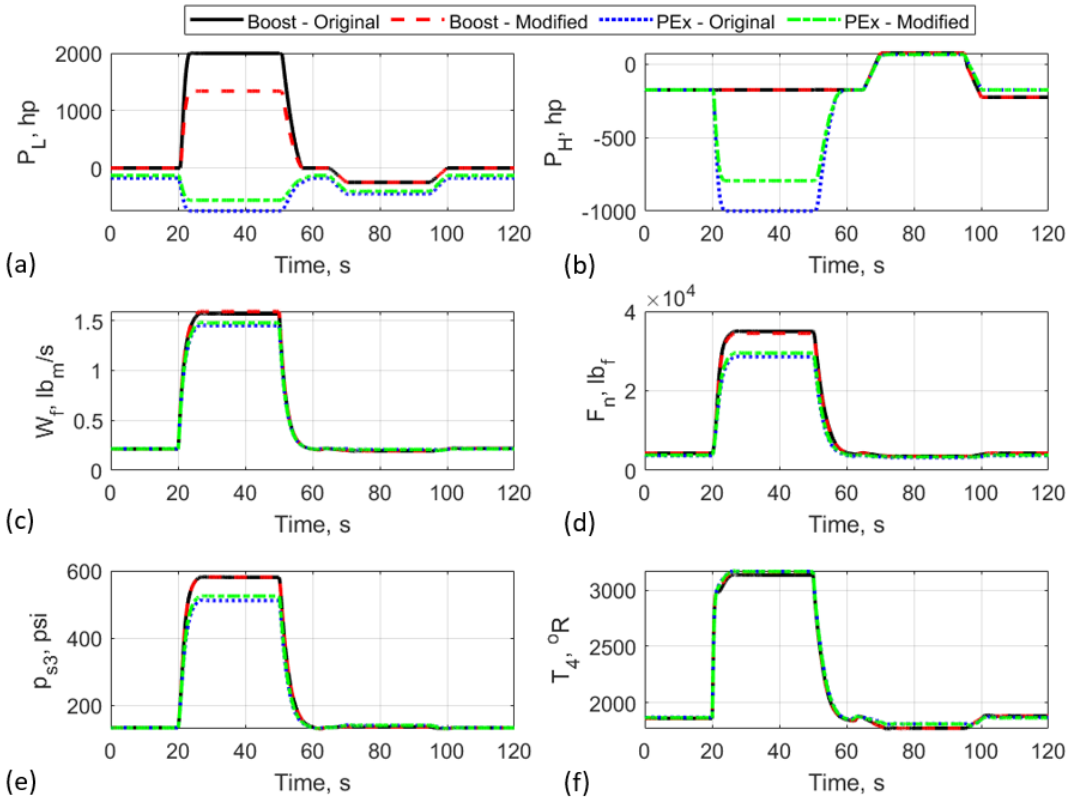

Figure 20. Select simulation results with and without power schedule modifications

the generic transient limit logic option was enabled. No other changes were made to the controller. The model was simulated for boost and PEx at SLS conditions using the input profiles given in Fig. 12. A subset of the results are shown in Fig. 20. As can be seen, the model runs seamlessly with the new power schedules. As to be expected, the reduction in boost results in a slight reduction in thrust and the reduction in power extraction results in a slight increase in engine thrust. All solutions share a similar maximum turbine inlet temperature that limits the operation of the engine.

V. Conclusions

The Advanced Geared Turbofan 30,000lb_f – electrified (AGTF30-e) is a recent addition to NASA's legacy in the development of airbreathing propulsion modeling. The engine model is representative of a relevant futuristic propulsion system and incorporates various features including electrification options and options for integrating an electric power system with turbomachinery. The purpose of the model is to facilitate research through supporting modeling and simulation studies. The model could be used as is or tailored to support specifically focused studies. The topics of research could vary but might include: engine electrification, investigation and optimization of engine and electric machine integration options, transient analysis, control strategy development and testing, etc. Within this paper, the AGTF30-e has been demonstrated through various simulation scenarios. The results demonstrate the impact of boost and power extraction (PEx). The benefits of electric power transfer (EPT) and turbine electrified energy management (TEEM) were also illustrated. A non-trivial concept for engine and electric machine integration has been incorporated and the results suggest further investigation is warranted. The results not only illustrate a propulsion system capable of running with various options, but a controller capable of achieving realistic behavior. The examples presented should provide the reader with a sense of what the AGTF30-e is capable of, and how it might be used to facilitate related research. Future work could include items such as enhancement of the electrical power system model and optimization of the electrical power system configuration and mechanical integration solution.

Appendix

The AGTF30-e has a transient model of a VEATE PGB. The contents of this appendix provide the mathematical expressions necessary for modeling the shaft dynamics and computing the effect of the gearbox.

Parameter definitions:

- J_c = inertia of the carrier (may include reflected inertias of any directly connected components including the engine shafts or EMs)
- J_p = inertia of a single planet gear (may include reflected inertias of any directly connected EMs)
- J_r = inertia of the ring gear (may include reflected inertias of any directly connected components including the engine shafts or EMs)
- J_s = inertia of the sun gear (may include reflected inertias of any directly connected components including the engine shafts or EMs)
- m_p = mass of a single planet gear
- n_p = number of planet gears
- r_p = radius of the planet gears
- r_r = radius of the ring gear
- r_s = radius of the sun gear
- τ_c = torque applied on the carrier
- τ_p = torque applied on each planet
- τ_r = torque applied on the ring gear
- τ_s = torque applied on the sun gear

Simplifying variables:

$$\lambda = \frac{1}{m_p(r_s + r_p)} \qquad \zeta = \frac{1}{J_c} n_p (r_s + r_p) \qquad \Theta = \frac{{r_p}^2}{J_p} + n_p \frac{{r_s}^2}{J_s}$$

$$\xi = \frac{{r_p}^2}{J_p} + n_p \frac{{r_r}^2}{J_r} \qquad \varphi = -\Theta - \frac{{r_p}^2}{J_p} \qquad \sigma = \frac{1}{\varphi}\left(r_s \zeta + \Theta\left(1 + \frac{\zeta}{\lambda}\right)\right)$$

$$\eta = \frac{1}{\varphi}\left(\frac{r_s}{J_c} + \frac{\Theta}{\lambda}\frac{1}{J_c}\right) \qquad \alpha = -\frac{r_s}{J_s}\frac{1}{\varphi}\left(\frac{{r_p}^2}{J_p} + \xi\right) \qquad \upsilon = \frac{r_p}{J_p}\left[-\frac{1}{\varphi}\frac{{r_p}^2}{J_p} + \left(-\frac{\xi}{\varphi} - 1\right)\right]$$

$$\gamma = -\frac{{r_p}^2}{J_p}\left(\sigma + \left(1 + \frac{\zeta}{\lambda}\right)\right) - \sigma\xi + r_r\zeta \qquad \kappa = \sigma + \left(1 + \frac{\zeta}{\lambda}\right) \qquad \beta = \frac{{r_p}^2}{J_p}\left(\eta + \frac{1}{\lambda}\frac{1}{J_c}\right) + \eta\xi - \frac{r_r}{J_c}$$

Forces:

Force at the planet gear and carrier interface: $f_{pc} = \frac{\alpha}{\gamma}\tau_s + \frac{\beta}{\gamma}\tau_c + \frac{1}{\gamma}\frac{r_r}{J_r}\tau_r + \frac{\upsilon}{\gamma}\tau_p$

Force at the sun gear and planet gear interface: $f_{sp} = \left(\frac{\kappa\alpha}{\gamma} - \frac{1}{\varphi}\frac{r_s}{J_s}\right)\tau_s + \left(\frac{\kappa\beta}{\gamma} + \eta + \frac{1}{\lambda}\frac{1}{J_c}\right)\tau_c + \frac{\kappa}{\gamma}\frac{r_r}{J_r}\tau_r + \left(\frac{\kappa\upsilon}{\gamma} - \frac{1}{\varphi}\frac{r_p}{J_p}\right)\tau_p$

Force at the ring gear and planet gear interface: $f_{pr} = \left(-\frac{\sigma\alpha}{\gamma} + \frac{1}{\varphi}\frac{r_s}{J_s}\right)\tau_s - \left(\frac{\sigma\beta}{\gamma} + \eta\right)\tau_c - \frac{\sigma}{\gamma}\frac{r_r}{J_r}\tau_r - \left(\frac{\sigma\upsilon}{\gamma} + \frac{1}{\varphi}\frac{r_p}{J_p}\right)\tau_p$

Effective Inertia (as seen by the component):

$$J_{s,Eff} = \frac{J_s}{1 - n_p r_s\left(\frac{\kappa\alpha}{\gamma} - \frac{1}{\varphi}\frac{r_s}{J_s}\right)} \qquad J_{r,Eff} = \frac{J_r}{1 + n_p\frac{\sigma}{\gamma}\frac{{r_r}^2}{J_r}} \qquad J_{c,Eff} = \frac{J_c}{1 + n_p(r_s + r_p)\frac{\beta}{\gamma}}$$

Torque coefficients:

Impact on ➡ / ⬇ τ input on	Sun gear	Ring gear	Carrier
Sun gear	$C_{ss} = 1$	$C_{rs} = \frac{n_p r_r\left(\frac{\sigma\alpha}{\gamma} - \frac{1}{\varphi}\frac{r_s}{J_s}\right)}{1 + n_p\frac{\sigma}{\gamma}\frac{{r_r}^2}{J_r}}$	$C_{cs} = \frac{n_p(r_s + r_p)\alpha}{\gamma + n_p(r_s + r_p)\beta}$
Ring gear	$C_{sr} = -\frac{n_p r_s\frac{\kappa}{\gamma}\frac{r_r}{J_r}}{1 - n_p r_s\left(\frac{\kappa\alpha}{\gamma} - \frac{1}{\varphi}\frac{r_s}{J_s}\right)}$	$C_{rr} = 1$	$C_{cr} = \frac{n_p(r_s + r_p)}{\gamma + n_p(r_s + r_p)\beta}\frac{r_r}{J_r}$
Carrier	$C_{sc} = -\frac{n_p r_s\left(\frac{\kappa\beta}{\gamma} + \eta + \frac{1}{\lambda}\frac{1}{J_c}\right)}{1 - n_p r_s\left(\frac{\kappa\alpha}{\gamma} - \frac{1}{\varphi}\frac{r_s}{J_s}\right)}$	$C_{rc} = \frac{n_p r_r\left(\frac{\sigma\beta}{\gamma} + \eta\right)}{1 + n_p\frac{\sigma}{\gamma}\frac{{r_r}^2}{J_r}}$	$C_{cc} = 1$
Planet Gears	$C_{sp} = \frac{n_p r_s\left(\frac{\kappa\upsilon}{\gamma} - \frac{1}{\varphi}\frac{r_p}{J_p}\right)}{1 - n_p r_s\left(\frac{\kappa\alpha}{\gamma} - \frac{1}{\varphi}\frac{r_s}{J_s}\right)}$	$C_{rp} = \frac{n_p r_r\left(\frac{\sigma\upsilon}{\gamma} + \frac{1}{\varphi}\frac{r_p}{J_p}\right)}{1 + n_p\frac{\sigma}{\gamma}\frac{{r_r}^2}{J_r}}$	$C_{cp} = \frac{n_p(r_s + r_p)\upsilon}{\gamma + n_p(r_s + r_p)\beta}$

Acknowledgments

The author would like to acknowledge the Transformational Tools & Technologies (TTT) project under the NASA Aeronautics Research Mission Directorate (ARMD) that has supported this work.

References

[1] Jansen, R. H., Bowman, C., Jankovsky, A., Dyson, R., and Felder, J., "Overview of NASA Electrified Aircraft Propulsion Research for Large Subsonic Transports," 53rd AIAA/SAE/ASEE Joint Propulsion Conference, Atlanta, GA. July 10-12, 2017.

[2] Jaw, L., and Mattingly, J., *Aircraft Engine Controls: Design, System Analysis, and Health Monitoring*, AIAA Educational Series, AIAA, Virginia, 2009, pp.13.

[3] Lytle, J., "The Numerical Propulsion System Simulation: An Overview," NASA/TM-2000-209915, 2000.

[4] Chapman, J., Lavelle, T., May, R., Litt, J., and Guo, T.-H., "Toolbox for the Modeling and Analysis of Thermodynamic Systems (T-MATS) User's Guide," NASA TM-2014-216638, 2014.
[5] Chapman, J., Litt, J., "Control Design for an Advanced Geared Turbofan Engine," AIAA Joint AIAA/ASME/SAE/ASEE Joint Propulsion Conference, Atlanta, GA, 2017.
[6] Jones, S., Haller, W., Tong, M., "An N+3 Technology Level Reference Propulsion System," NASA/TM-2017219501, 2017.
[7] Kratz, J. L., Culley, D. E., and Thomas, G. L., "Thermal Modeling of an Advanced Geared Turbofan for Distributed Engine Control Applications," 2018 Joint Propulsion Conference, Cincinnati, OH. July 9-11, 2018.
[8] Kratz J. L., and Chapman, J. W., "Active Turbine Tip Clearance Control Trade Space Analysis of an Advanced Geared Turbofan Engine," 2018 Joint Propulsion Conference, Cincinnati, OH. July 9-11, 2018.
[9] Kratz, J. L., Culley, D. E., and Thomas, G. L., "A Control Strategy for Turbine Electrified Energy Management," AIAA Propulsion and Energy Forum, Indianapolis, IN August 19-22, 2019.
[10] Kratz, J. L., Culley, D. E., and Thomas, G. L., "Evaluation of Electrical System Requirements for Implementing Turbine Electrified Energy Management," AIAA Propulsion and Energy Forum, Indianapolis, IN August 19-22, 2019.
[11] Kratz, J. L., and Culley, D. E., "Exploration of the Versatile Electrically Augmented Turbine Engine Gearbox Concept," AIAA Propulsion and Energy Forum. Virtual Event. August 9-11, 2021.
[12] Kratz, J. L., "Transient Optimization of a Gas Turbine Engine," AIAA SciTech Forum, National Harbor, MD. January 23-27, 2023.
[13] Kratz J. L., Culley, D. E., and Lehan, J., " Transient Optimization for the Betterment of Turbine Electrified Energy Management," AIAA SciTech Forum, National Harbor, MD. January 23-27, 2023.
[14] Khalid, S. J., and Diegelman, J., "Improving Turbofan Transient Characteristics with Multivariable Geometry Closed Loop Control," AIAA Propulsion and Energy Forum, virtual event, August 24-28, 2020.
[15] Khamvilai, T., Pakmehr, M., Lu, G., Yang, Y., Feron, E., and Behbahani, A., "Hardware-in-the-Loop Simulation Testbed Development for Distributed Turbine Engine Control Systems," AIAA SciTech Forum, San Diego, CA. January 3-7, 2022.
[16] Buescher, H. E., Culley, D. E., Bianco, S. J., Connolly, J. W., Dimston, A. E., Saus, J. R., Theman C. J., Horning M. A., and Purpera, N. C., "Hybrid-Electric Aero-Propulsion Control Laboratory: Overview and Capability," AIAA SciTech Forum, National Harbor, MD. January 23-27, 2023.
[17] Bianco, S., Kratz, J. L., Culley D. E., Horning, M., Sachs-Wetstone, J. J., and Connolly, J. W., "Hybrid-Electric Aero-Propulsion Control Testbed Results with Energy Storage," AIAA Aviation Forum, San Diego, CA. June 12-16, 2023.
[18] Sachs-Wetstone, J., Bianco, S., Kratz, J. L., Horning, M., Amthor, A., Connolly, J. W., "Hybrid-Electric Aero-Propulsion Control Testbed Results," AIAA Aviation Forum, San Diego, CA. June 12-16, 2023.
[19] Yang, X., Jian, M., Xu, Q, Dong, W., "Turbofan engine performance prediction methodology integrated high-fidelity secondary air system models, Sage Journals, Vol. 237, Issue 5. September 21, 2022.
[20] Yang, X., Jian, M., Dong, W., Xu, Q., "Simulation of the secondary air system of turbofan engines: Insights from 1D-3D modeling," Chinese Journal of Aeronautics, Vol 36, Issue 1, Pg. 231-245, January 2023.
[21] Chao, M. A., Adey, B. T., Fink, O, "Implicit supervision for fault detection and segmentation of emerging fault types with Deep Variational Autoencoders," Elsevier Journal of Neurocomputing, Vol. 454, Pg. 324-338, September 24, 2021.
[22] Bradley, M. K., Droney, C. K., "Subsonic Ultra Green Aircraft Research: Phase II – Volume II – Hybrid Electric Design Exploration," NASA CR-218704. 2015.
[23] Welstead, J. R., Felder, J. L., "Conceptual Design of a Single-Aisle Turboelectric Commercial Transport with Fuselage Boundary Layer Ingestion," AIAA SciTech Forum, San Diego, CA. 2016.
[24] Enalou, H. B., Bozhko, S., "Electric Power Transfer Concept for Enhanced Performance of the More Electric Engine," Journal of Engineering for Gas Turbines and Power, Vol. 143, Issue 9, April 19, 2021.
[25] Enalou, H. B., Bozhko, S., "Performance Improvement of Turbofans by Electric Power Transfer (EPT)," Journal of Turbomachinery, Vol. 142, Issue 11, July, 2020.
[26] Culley, D., Kratz, J., and Thomas, G., "Turbine Electrified Energy Management (TEEM) for Enabling More Efficient Engine Designs," AIAA 2018-4798, Joint Propulsion Conference, Cincinnati, OH, July, 2018.
[27] May, R., Csank, J., Litt, J., and Guo, T.-H., "Commercial Modular Aero-Propulsion System Simulation 40k (C-MAPSS40k) User's Guide, NASA TM-2010-216831, 2010.
[28] Kratz, J., and Simon, D., "Failure Behavior and Control Based Mitigation for a Parallel Hybrid Propulsion System," AIAA SciTech Forum, Orlando, FL. January 8-12, 2023.